Journal of Cleaner Production 426 (2023) 139032

Contents lists available at ScienceDirect

Journal of Cleaner Production

journal homepage: www.elsevier.com/locate/jclepro

Influence of urban extent discrepancy on the estimation of surface urban heat island intensity: A global-scale assessment in 892 cities

Qiquan Yang [a,b,c], Yi Xu [a,*], Xiaohua Tong [b,c,**], Ting Hu [d,***], Yue Liu [e], T.C. Chakraborty [f], Rui Yao [g], Changjiang Xiao [b,c], Shurui Chen [b], Zonghan Ma [h]

[a] State Key Laboratory of Lunar and Planetary Sciences, Macau University of Science and Technology, Macau, China
[b] College of Surveying & Geo-Informatics, Tongji University, Shanghai, 200092, China
[c] The Shanghai Key Laboratory of Space Mapping and Remote Sensing for Planetary Exploration, Tongji University, Shanghai, 200092, China
[d] School of Remote Sensing and Geomatics Engineering, Nanjing University of Information Science and Technology, Nanjing, 210044, China
[e] Guangzhou Institute of Geography, Guangdong Academy of Sciences, Guangzhou, 510070, China
[f] Atmospheric Sciences and Global Change Division, Pacific Northwest National Laboratory, Richland, WA, USA
[g] School of Remote Sensing and Information Engineering, Wuhan University, Wuhan, 430079, China
[h] State Key Laboratory of Remote Sensing Science, Aerospace Information Research Institute, Chinese Academy of Sciences, Beijing, 100101, China

ARTICLE INFO

Handling Editor: Cecilia Maria Villas Bôas de Almeida

Keywords:
SUHI
Urban definition
Impervious surface
Quantification
Globe

ABSTRACT

The estimation of surface urban heat island intensity (SUHII) is crucial for studying the urban thermal environment, which is influenced not only by the commonly known definition of rural reference but also by the delineation of urban extent. Existing studies relies on various urban extent products defined in different ways, and the influence of urban extent discrepancy (UED) on SUHII estimates still remains unclear. In this study, we collected five open-source global urban extent products (GUEPs) for the year 2015 and corresponding daily land surface temperature (LST) observations (MYD11A1). Based on these products, we quantified the UED-induced uncertainty in SUHII estimates by comparing absolute difference ($\Delta SUHII_{AD}$) and relative difference ($\Delta SUHII_{RD}$) in SUHII among GUEPs across 892 global cities. Besides, we introduced an ISF-constrained (ISF–C) method to reduce SUHII differences among GUEPs by constraining the impervious surface fraction (ISF) within urban and rural extents. The results show that urban extents delineated by different GUEPs are not consistent, leading to their difference in ISF as well as LST, which in turn causes uncertainties in the estimated SUHII. On average for global cities, the annual daytime and nighttime $\Delta SUHII_{AD}$ are 0.46 ± 0.02 °C (mean ± 95% confidence interval) and 0.24 ± 0.01 °C, with corresponding $\Delta SUHII_{RD}$ of 42.0 ± 2.7% and 35.2 ± 2.3%, respectively. The UED-induced uncertainty in SUHII estimates varies among climate zones, and the annual daytime $\Delta SUHII_{RD}$ averaged for cities located in the arid zone reaches up to 60.8 ± 6.6%, which is nearly twice as high as that in other climate zones. More importantly, both $\Delta SUHII_{AD}$ and $\Delta SUHII_{RD}$ show lower values when using the ISF-C method, implying the effectiveness of this method. This study highlights the non-negligible impact of UED on the estimation of SUHII, which requires more attention due to the inconsistency of urban extents among current products.

1. Introduction

The urban heat island (UHI) effect refers to the phenomenon where the temperature in urban areas is higher than that in rural areas. The temperature alteration induced by the UHI effect is of concern due to its impacts on vegetation phenology, soil environment, air quality, and health of residents in cities (Chen et al., 2015; Liu et al., 2021; Rizwan et al., 2008; Zhou et al., 2016b). The UHI intensity (i.e., the average temperature difference between urban and rural areas) is a typical indicator of the UHI effect, and has been widely used in various studies (Hu et al., 2022; Rizwan et al., 2008; Schwarz et al., 2011; Zhou et al., 2018). Therefore, accurate estimation of the UHI intensity is essential

* Corresponding author.
** Corresponding author. College of Surveying & Geo-Informatics, Tongji University, Shanghai, 200092, China.
*** Corresponding author.
E-mail addresses: yixu@must.edu.mo (Y. Xu), xhtong@tongji.edu.cn (X. Tong), hutingrs@nuist.edu.cn (T. Hu).

https://doi.org/10.1016/j.jclepro.2023.139032
Received 17 June 2023; Received in revised form 14 September 2023; Accepted 25 September 2023
Available online 26 September 2023

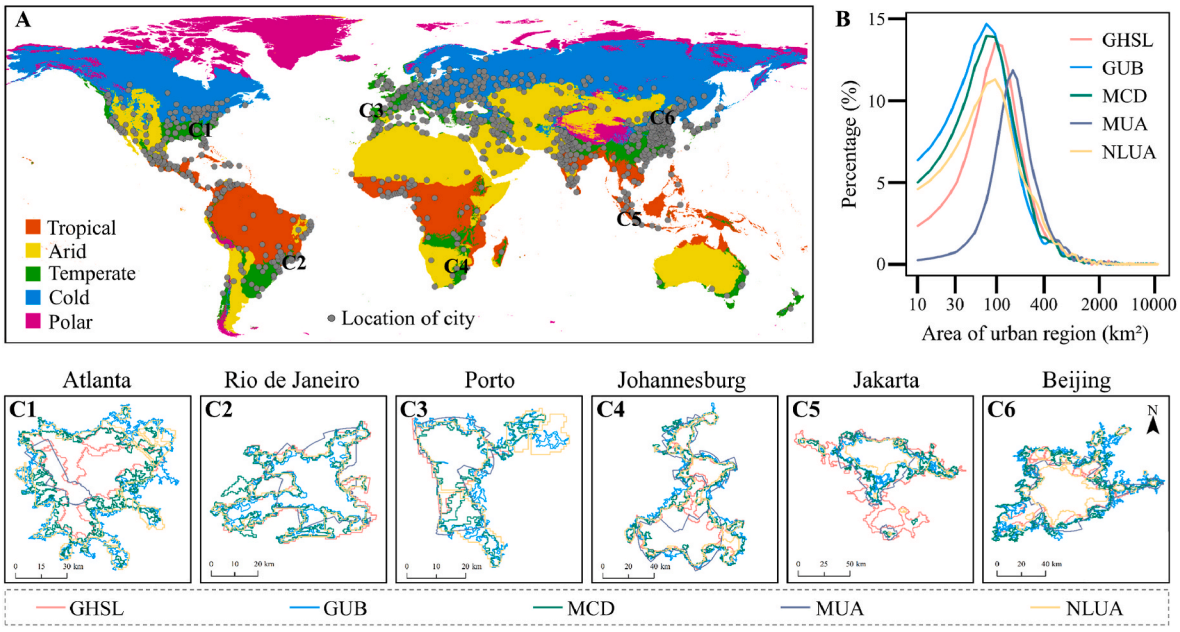

Fig. 1. Location of 892 global cities and their urban extent discrepancy. (A) Global map of the selected 892 cities and the climate zones. (B) Frequency distribution of the area of urban extents for the 892 cities corresponding to the five global urban extent products. (C1–C6) Examples of urban extent discrepancy in 6 typical cities.

for better understanding the urban thermal environment.

Traditional studies based on in-situ air temperature observations have shown that the UHI intensity can be significantly influenced by the selection of urban and/or rural stations (Jin, 2012; Mohsin and Gough, 2012). The development of thermal infrared remote sensing technology allows us to calculate the surface UHI intensity (SUHII) with the help of spatially continuous land surface temperature (LST) data (Zhou et al., 2018). The LST-based SUHII can avoid the limitation of sparse distribution of in-situ stations, but still requires the delineation of urban extents and their rural references (Li et al. 2018, 2019a, 2022; Liu et al., 2023; Yao et al., 2018a; Yang et al., 2023). Existing studies have mostly focused on the uncertainties caused by different definitions of the rural reference. For instance, through an analysis of 100 Chinese cities, Li et al. (2019a) found the variation in SUHII induced by rural reference discrepancy exceeded 0.5 K in a large number of cities. Besides, a global analysis by Li et al. (2022) pointed out that the daytime SUHII difference caused by different rural definitions reached 0.62 K, accounting for 42% of the global average SUHII.

The estimation of SUHII can be influenced not only by the rural reference definition but also potentially by the urban extent discrepancy (UED), for the following two reasons. First, the UED can lead to direct variations in land cover within urban areas, potentially influencing the average urban LST and introducing uncertainties in the SUHII estimates. Taking impervious surface, the most typical land cover in cities, as an example, its proportion generally decreases along the urban-rural gradients (Jia and Zhao, 2019). Hence, a smaller urban extent is often associated with a higher percentage of impervious surfaces within the urban area, which in turn often leads to elevated urban LST and corresponding estimated SUHII (Imhoff et al., 2010; Zhou et al., 2016a). Second, the UED can lead to changes in the corresponding rural reference areas, since the definition of rural reference generally relies on the central urban area. For instance, numerous studies have employed the equal-area buffer located in close proximity to the central urban area as the corresponding rural reference (Peng et al., 2012; Yang et al., 2017; Yao et al., 2018b; Zhou et al., 2014). Obviously, the UED will cause variations in rural references, and further influence rural average LST and the estimated SUHII.

In existing studies, there are generally two ways to access the urban extents for estimating SUHII. In the first one, researchers independently extracted the urban extents based on their own criteria. Zhou et al. (2014) extracted high-intensity (>50%) built-up polygons, and aggregated them with a distance of 2 km (km) to form the urban extents. Cao et al. (2016) manually selected 3 × 3 pixels in the center of the city, and regarded the patch formed by these pixels as the urban extent. The cases above show that current studies differ greatly in terms of urban definition, which will inevitably lead to the differences in the extracted urban extents. In addition, self-extraction of urban extents can greatly increase the computational workload and create challenges for large-scale multi-city studies. In view of the above situations, most studies have opted for the alternative way of directly utilizing existing products to determine urban extents. For instance, based on the Moderate-resolution Imaging Spectroradiometer (MODIS) land cover products (MCD12Q1), Yao et al. (2019) identified the category of "urban and built-up lands" as the urban extent, and analyzed the SUHII trend and its drivers in 397 global cities. Similarly, based on the MCD12Q1 product, Chakraborty and Lee (2019) quantified the SUHII as the average LST difference between "urban and built-up lands" and other land cover types, and applied it to more than 9500 cities worldwide. In addition to the MODIS land cover products, the Global Human Settlement Layer (GHSL) products have also been used in the SUHI studies. For example, Venter et al. (2021) aggerated the low- and high-density urban pixels from the GHSL product to obtain urban extents, and analyzed the spatiotemporal patterns of SUHII in 342 European cities. Similarly, Chakraborty et al. (2022) defined urban extents as the contiguous low- and high-density urban patches when analyzing the European heat stress. Recently, Li et al. (2020b) published a free-access product of the Global Urban Boundary (GUB), which has been widely used to get urban extents due to its advantages of good accuracy and high resolution. For example, Liu et al. (2022) analyzed the diurnal and seasonal patterns of the SUHII in more than 2000 global cities by using the urban extents selected from the GUB product. Du et al. (2021) compared the SUHII with the canopy UHI intensity in 366 global cities based on the urban extents from the GUB product. Besides, the nighttime light intensity is a good indicator for human activities, and can provide important information for urban extent delineations. As a result, the nighttime light observations and corresponding urban extent products have been widely used in SUHI studies (Li et al., 2020a; Sun et al., 2020; Zhang et al., 2014). Finally, some studies have produced urban extent products from the perspective

Table 1
The main abbreviations in this paper.

Type	Abbreviation	Definition
High-frequency phrases	GUEP	Global urban extent product
	ISF	Impervious surface fraction
	LST	Land surface temperature
	MODIS	Moderate-resolution Imaging Spectroradiometer
	SUHII	Surface urban heat island intensity
	UED	Urban extent discrepancy
	UHI	Urban heat island
Global urban extent products	GHSL	Global Human Settlement Layer
	GUB	Global Urban Boundary
	MCD	MODIS land cover product datasets (MCD12Q1)
	MUA	Morphological Urban Area
	NLUA	Nighttime-Light-based Urban Area
Indicators and parameters	DiffISF	Urban-rural difference in ISF
	ΔDiffISF	Difference in DiffISF between GUEPs
	ISF-C	ISF-constrained
	ISF_U	The threshold of minimum ISF in urban extents for the ISF-C method
	ISF_R	The threshold of maximum ISF in rural extents for the ISF-C method
	$\Delta SUHII_{AD}$	Absolute difference in SUHII between GUEPs
	$\Delta SUHII_{RD}$	Relative difference in SUHII between GUEPs

of the physical morphology for cities (Taubenböck et al., 2019; Wang et al., 2022), which can provide new insights for heat island studies considering the potential impact of the urban form on SUHII (Zhou et al., 2017).

In summary, various urban extent products were produced in different ways, and have been widely used in urban thermal environment studies. The difference in the data and methods among existing products can lead to discrepancy in urban extents, and probably influence the estimated SUHII. For example, Imhoff et al. (2010) compared LST differences between urban core and non-core areas with rural reference areas in 38 most populous cities in North America, and their results showed that the SUHII calculated based on urban core areas was higher than the SUHII calculated based on urban non-core areas. Similarly, Zhou et al. (2016a) noted substantial variations in the estimated SUHII resulting from different definitions of urban areas in a study covering 32 cities in China. However, there is still a lack of comprehensive, large-scale (such as global) quantitative analyses to assess influence of UED (i.e. urban extent discrepancy) on the estimation of SUHII. Consequently, the uncertainty in SUHII estimates resulting from UED (termed as the "UED-induced uncertainty in SUHII estimates"), as well as potential approaches to mitigate this uncertainty, remains unclear.

Therefore, this study presents a global-scale quantitative analysis of the influence of UED on the estimation of SUHII. The aims of this study include: 1) quantify the UED-induced uncertainty in SUHII estimates; 2) analyze its spatiotemporal variation; 3) and explore possible methods to reduce the UED-induced uncertainty in SUHII estimates. The data used in this study include MODIS LST products (MYD11A1), five global urban extent products, and other ancillary data (further details are available in the subsequent section). All of the data products were acquired in the year of 2015 (with the exception of elevation data and climate map) and encompass a total of 892 global cities (Fig. 1(A)). Table 1 lists the main abbreviations used in this paper to make the paper easy to understand.

2. Data and methods

2.1. Data

2.1.1. Global urban extent products

In this study, we considered a total of five publicly available global urban extent products (GUEPs): the Global Human Settlement Layer (GHSL) produced by the European Space Agency, the Global Urban Boundary (GUB) produced by Li et al. (2020b), the MODIS land cover product (MCD12Q1, referred as MCD) from the United States Geological Survey, the global Morphological Urban Area (MUA) shared by Taubenböck et al. (2019), and the global datasets of Nighttime-Light-based Urban Area (NLUA) published by Zhao et al. (2022). Table 2 provides brief descriptions of all the GUEPs, and more detail information can be found in Text A.1 of Supplementary Material.

Table 2
Summary of datasets used in this study.

Type	Product (abbreviation)	Source	Usage
LST data	MODIS LST product (MYD11A1)	United States Geological Survey (USGS)	Calculation of SUHII
Global urban extent products	Global Human Settlement Layer (GHSL)	European Space Agency	Delimitation of urban extents in global cities
	Global Urban Boundary (GUB)	Li et al. (2020b)	
	MODIS land cover product (MCD)	USGS	
	Morphological Urban Area (MUA)	Taubenböck et al. (2019)	
	Nighttime-Light-based Urban Area (NLUA)	Zhao et al. (2022)	
Auxiliary data	Global 30 arc-second elevation	USGS	Remove the influence of topographic relief
	Global surface water dataset	Joint Research Center of the European Commission	Remove the influence of water bodies
	Global impervious surface area dataset	Huang et al. (2022)	Construction of the ISF-C method
	Köppen–Geiger climate map	Beck et al. (2018)	Determination of the climate zone of cities

In order to fairly compare the urban extents of the above five GUEPs, we standardized the acquisition year of the GUEPs to 2015, and performed the subsequent processing. First, we converted raster into vector to get the urban extent patches, eliminated inner holes of each patch, and removed isolated patches smaller than 1 km^2. Second, we combined all the five GUEPs, and merged patches that were spatially overlapped. Third, we searched for isolated patches that must be merged by all the five GUEPs from the global merged map, and a total of 892 isolated patches were obtained (Fig. 1(A)). The *i*th selected patch is labelled as M_i, indicating the potentially maximum urban extent of the *i*th selected city. Finally, we separately extracted all the patches corresponding to each GUEP within the spatial extent of M_i. For the *i*th city, suppose that the extracted patches corresponding to the *k*th GUEP is M_{ik}, and the M_{ik} refers to the urban extent of the *k*th GUEP in the *i*th city.

As depicted in Fig. 1(B), there are obvious differences in the distribution curves of the area of urban extents corresponding to different GUEPs. The average area of urban extents of 892 cities reaches 450.6 ± 46.6 km^2 for MUA, followed by NLUA (393.6 ± 44.4 km^2), GHSL (391.5 ± 48.9 km^2), GUB (356.4 ± 51.6 km^2), and MCD (351.5 ± 48.4 km^2). The difference in area reveals the inconsistency of the urban extents delineated by the different GUEPs. The UED (i.e., urban extent discrepancy) for six typical cities is shown in Fig. 1(C). Since the SUHII is defined as the average LST difference between urban and surrounding rural areas, the UED will inevitably have an impact on the quantified SUHII.

2.1.2. Land surface temperature

The LST data used in this study were derived from the MODIS

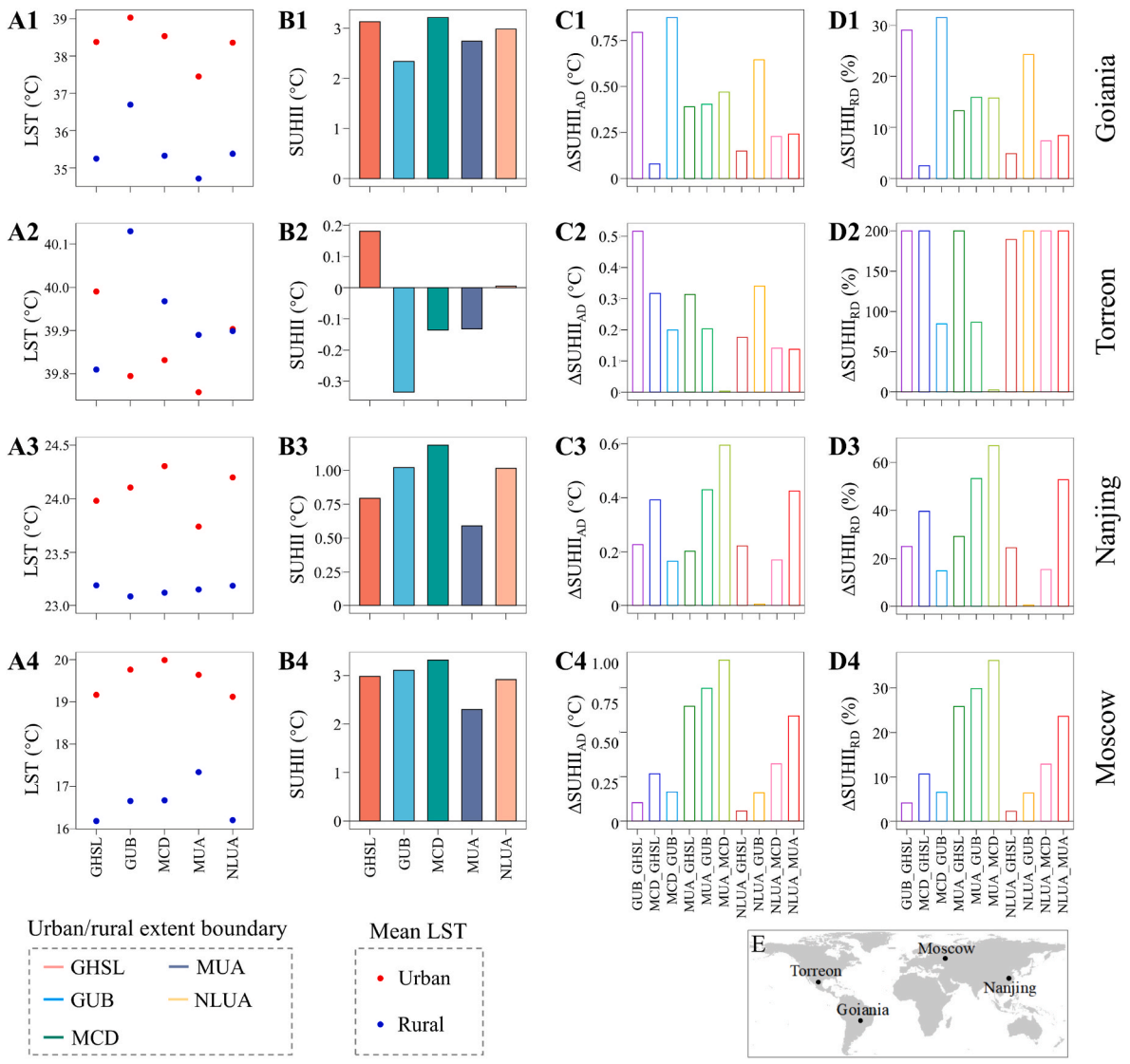

Fig. 2. Examples of the SUHII uncertainty caused by urban extent discrepancy. (A1-A4) Mean values of annual daytime LST in urban and rural areas. (B1–B4) Annual daytime SUHII estimated by different global urban extent products (GUEPs). (C1–C4) Absolute difference in SUHII ($\Delta SUHII_{AD}$) for each GUEP pair. (D1-D4) Relative difference in SUHII ($\Delta SUHII_{RD}$) for each GUEP pair. The four sample cities (Goiania, Torreon, Nanjing, Moscow) belong to different climate zones (tropical, arid, temperate, cold), and their locations are marked on the map in the bottom-right corner.

version-6 LST product (MYD11A1). This product provides per-pixel LST measurements globally, with a spatial resolution of 1 km, for both daytime (~13:30) and nighttime (~1:30) periods. Previous studies proved the overall good accuracy of the MODIS LST product (Duan et al., 2018; Wan, 2014). Consistent with the GUEPs, we included the MYD11A1 LST images covering the entire year of 2015. The MODIS LST dataset, marked by diverse degrees of precision, has been distinctly differentiated using a quality control (QC) band. Each QC value has been encoded as an 8-bit binary number, encompassing four distinct flags denoting the mandatory QA (quality assurance), data quality, emissivity error, and LST error. Pixels flagged with a mandatory QA values of "10" or "11" were excluded from analysis because the LST of these pixels were invalid due to cloud coverage. Besides, the LST pixels with errors higher than 3K were also filtered out (Lai et al., 2018). Then, these daily LST observations were annually and seasonally averaged. For northern (southern) hemisphere cities, the periods of summer and winter are June–August (December–February) and December–February (June–August), respectively.

2.1.3. Auxiliary data

Surface elevation data: The Global 30 Arc-Second Elevation is a global digital elevation model developed by the United States Geological Survey in collaboration with many research institutes worldwide (Miliaresis and Argialas, 1999). The digital elevation model was used to remove or reduce the effect of topographic relief on the estimation of SUHII.

Surface water data: The datasets of the global surface water can be freely accessed from the Joint Research Center of the European Commission. Validation results reveal that the overall accuracy of the global surface water datasets is good, with errors of omission less than 5% and commission less than 1% (Pekel et al., 2016). We used the maximum extent of global surface water in 2015 to remove the influence of water bodies on SUHII estimates.

Impervious surface data: The global impervious surface area is provided by Huang et al. (2022), which has a spatial resolution of 30 m and an F_1-score score of 0.935. We used this product for the year 2015 and calculated the impervious surface fraction (ISF) in a 1 km spatial grid to obtain the global ISF map. This data was used to construct possible strategies for mitigating the UED-induced uncertainty.

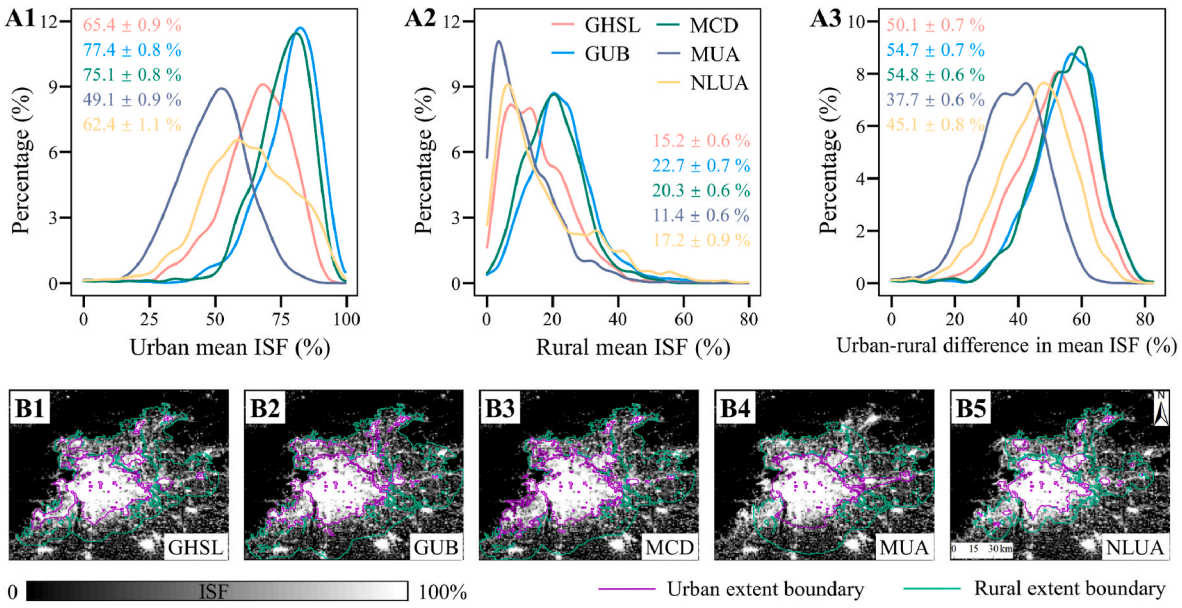

Fig. 3. Inconsistency of impervious surface fraction (ISF) among global urban extent products. (A1-A3) Frequency distribution of urban mean ISF, rural mean ISF, and urban-rural difference in mean ISF corresponding to the five global urban extent products. (B1–B5) Spatial distribution of ISF within urban and rural extents, taking the city of Beijing as an example.

Climatic classification data: The Köppen climate classification encompassing five primary climate zones based on precipitation and temperature patterns across the global terrestrial surface (Kottek et al., 2006). As shown in Fig. 1(A), the 892 cities of this study spread across four main climate zones, including tropical zone (155 cities), arid zone (210 cities), temperate zone (316 cities), and cold zone (211 cities), according to the publicly available Köppen–Geiger climate map (Beck et al., 2018).

2.2. Methods

2.2.1. Calculation of SUHII

The prerequisite for estimating SUHII is the delineation of urban and rural extents. The urban extents can be obtained from existing GUEPs, while the rural extents are generally obtained by constructing buffers around the central urban. Buffers are commonly created using two approaches: the distance-based method and the area-based method. In the distance-based approach, a buffer ring is formed around the central urban area at a specific distance (d) with a designated width (w). However, recent studies have shown variability in the choice of parameters for w and d, leading to significant uncertainties in estimating SUHII (Li et al., 2019a). The area-based method determines the rural extent as the neighboring buffer ring with a certain time of the urban size. Compared with the distance-based method, the area-based method has fewer parameters and is more suitable for studies with cities of different sizes (Chakraborty et al., 2021; Li et al. 2019a, 2022). Therefore, the area-based method was chosen for this study to define the rural reference. Considering the need to remove the areas covered by water bodies or disturbed by topographic relief (i.e., higher or lower than the median elevation of urban areas by 50 m), we defined the rural reference area as the neighboring buffer ring that is twice the size of the central urban area. In addition, we also defined rural area as the neighboring equal-area buffer and found similar results (Fig. A1).

A total of 892 cities were included in this study, and each city has five different urban extents derived from the corresponding GUEPs. For each city, the rural extent corresponding to every urban extent was obtained by the above method. Assuming the mean values of LST within urban extent and its corresponding rural extent are LST_{Urban} and LST_{Rural}, respectively, and the SUHII can be calculated by the following equation:

$$SUHII = LST_{Urban} - LST_{Rural} \quad (1)$$

2.2.2. Quantification of the UED-induced uncertainty in SUHII estimates

Based on the five GUEPs, we can obtain five sets of urban and rural extents and corresponding SUHII of the selected 892 cities. We calculated the SUHII difference between each GUEP pair, and used their absolute difference to measure the UED-induced uncertainty in SUHII estimates. For a given city, if the SUHII corresponding to any two sets of GUEPs are $SUHII_1$ and $SUHII_2$, then the absolute difference between them (denoted as $\Delta SUHII_{AD}$) can be expressed as the following equation:

$$\Delta SUHII_{AD} = |SUHII_1 - SUHII_2| \quad (2)$$

A larger $\Delta SUHII_{AD}$ indicates a higher UED-induced uncertainty in SUHII estimates. In addition to the absolute difference, we should also focus on the relative difference in SUHII. Here we use the percentage difference indicator to quantify the relative difference in SUHII (denoted as $\Delta SUHII_{RD}$), which can be expressed as the following equation:

$$\Delta SUHII_{RD} = \frac{|SUHII_1 - SUHII_2|}{(|SUHII_1| + |SUHII_2|)/2} \times 100\% \quad (3)$$

The $\Delta SUHII_{RD}$ ranges from 0 to 200%. When $\Delta SUHII_{RD}$ reaches 200%, it means the signs of $SUHII_1$ and $SUHII_2$ are opposite, implying a transition between heat and cold islands.

Paired combination of the five GUEPs and corresponding SUHIIs yields ten sets of $\Delta SUHII_{AD}$ or $\Delta SUHII_{RD}$. Fig. 2 shows urban extents and annual daytime $\Delta SUHII_{AD}$ and $\Delta SUHII_{RD}$ in four typical cities. It can be seen that the difference in urban extents causes a change in the urban and rural average LST, which in turn influences the estimated SUHII. More importantly, $\Delta SUHII_{AD}$ and $\Delta SUHII_{RD}$ differ greatly among cities and GUEP pairs. It is therefore necessary to make a more comprehensive analysis of the UED-induced uncertainty in SUHII estimates across global cities.

2.2.3. Methods to reduce the UED-induced uncertainty in SUHII estimates

The fundamental reason for the SUHII difference caused by UED is that changes in urban extents can pose a direct impact on both urban and rural land covers. Therefore, trying to reduce the land cover difference caused by changes in urban/rural extents is a potential way to reduce the UED-induced uncertainty in SUHII estimates. Based on this idea, we first

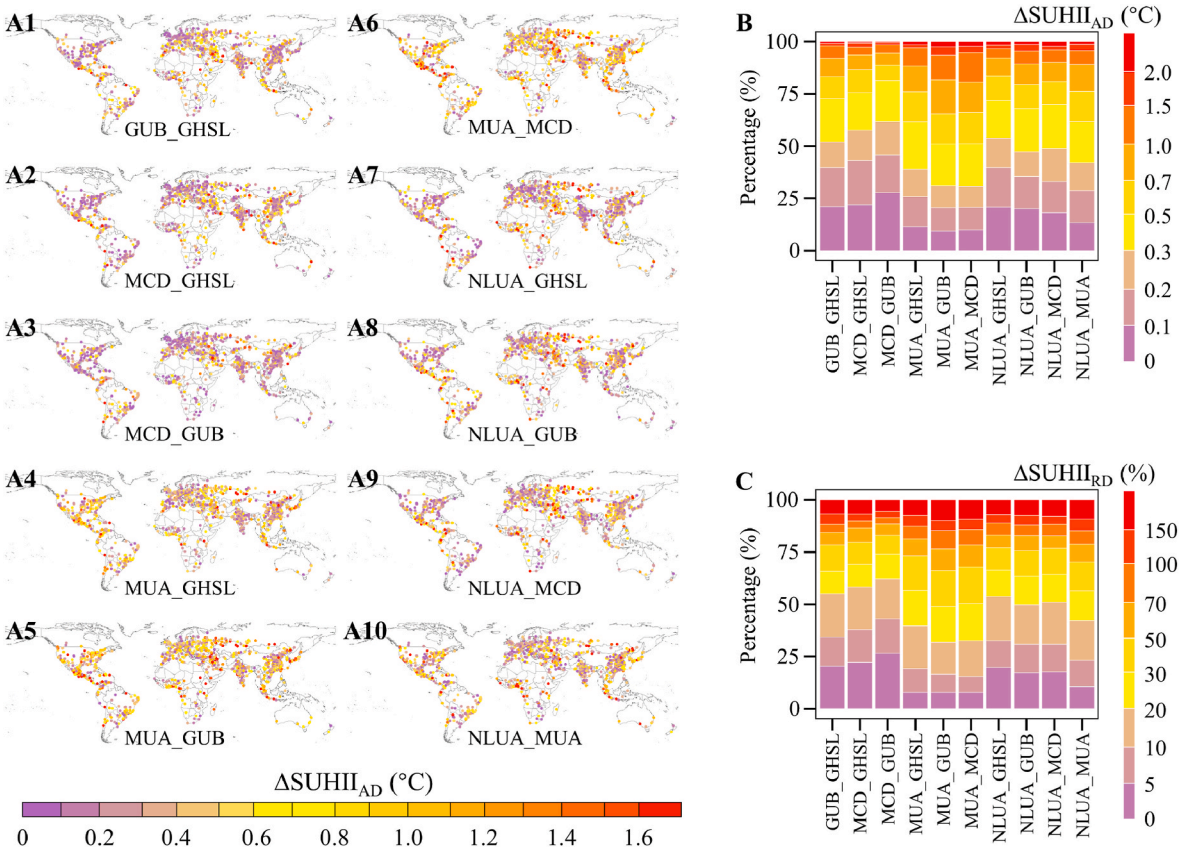

Fig. 4. Annual daytime $\Delta SUHII_{AD}$ and $\Delta SUHII_{RD}$ for global cities. (A1-A10) Spatial distributions of $\Delta SUHII_{AD}$. (B) Stacked frequency distributions of $\Delta SUHII_{AD}$. (C) Stacked frequency distributions of $\Delta SUHII_{RD}$. $\Delta SUHII_{AD}$ and $\Delta SUHII_{RD}$ represent absolute and relative differences in SUHII between global urban extent products, respectively.

turn our attention to the most typical urban land cover type, the impervious surface. Impervious surface fraction (i.e., ISF) reflects the degree of urbanization, and its distribution not only directly affects the ground cover, but also is closely related to the urban population and its heat source emissions (Huang et al., 2022). On average for the 892 cities, the mean ISF of urban (rural) areas reaches 77.4% (22.7%) for GUB, but only 49.1% (11.4%) for MUA. The UED-induced change in urban and/or rural ISF can result in the variation of urban-rural difference in ISF (DiffISF) (Fig. 3).

Considering the close relation between LST and ISF (Yang et al., 2021), the difference in DiffISF between GUEPs (referred as ΔDiffISF) is likely to be the key driver for the UED-induced uncertainty in SUHII estimates. Therefore, we designed an ISF-constrained (ISF–C) method, which is able to reduce the ΔDiffISF when estimating SUHII. The ISF-C method is based on the basic assumption that the ISF is generally higher in urban areas and lower in rural areas. The first is to screen urban and rural extents as follows: for urban extents, only pixels with the ISF greater than a certain threshold (ISF_U) are retained; for rural extents, only pixels with the ISF less than a certain threshold (ISF_R) are retained. Then, the average LST of the retained pixels within urban and rural extents are calculated separately, and their difference is the SUHII processed by the ISF-C method. According to previous SUHI studies (Imhoff et al., 2010; Li et al., 2019b; Zhang et al., 2014), the ISF within rural extents shall be less than 5%, so we set the ISF_R to 5%. In contrast, the lower limit of ISF within urban extents varies from study to study and generally includes values such as 25%, 50% and 75% (Imhoff et al., 2010; Zhou et al., 2016a). In this study, we set the ISF_U to 50%. Please refer to section 3.2 for the results of the other values of ISF_U.

To validate the ISF-C method, we conducted comparative analysis as follows. First, we estimated the SUHII corresponding to each GUEP processed by the ISF-C method in 892 global cities. Second, we calculated $\Delta SUHII_{AD}$ and $\Delta SUHII_{RD}$ the for all GUEP pairs using the SUHII obtained in the previous step. Finally, we compared $\Delta SUHII_{AD}$ and $\Delta SUHII_{RD}$ processed by the ISF-C method with the regular estimates. If the former is smaller than the latter, it indicates that our proposed ISF-C method is effective for reducing the UED-induced uncertainty in the estimation of SUHII.

3. Results

3.1. Spatiotemporal patterns of the UED-induced uncertainty in SUHII estimates

Figs. 4 and 5 show the spatial patterns of annual daytime and nighttime $\Delta SUHII_{AD}$ (i.e., absolute difference in SUHII) in 892 global cities. The annual daytime $\Delta SUHII_{AD}$ is greater than 0.5 °C in about one-third to one-half of the cities, with specific values related to GUEP pairs (Fig. 4(B)). On average for all cities, the annual daytime $\Delta SUHII_{AD}$ has a minimum value of 0.32 ± 0.02 °C (MCD_GUB, refers to the SUHII difference for GUEP pair of MCD and GUB, hereinafter), a maximum value of 0.62 ± 0.03 °C (MUA_GUB), and a mean value of 0.46 ± 0.02 °C (averages for all GUEP pairs) (Fig. 6(A1)).

In addition to the absolute difference in SUHII among GUEPs, we also focus on their relative difference (i.e., $\Delta SUHII_{RD}$). The annual daytime $\Delta SUHII_{RD}$ is larger than 10% in most cities (Fig. A2), accounting for 57% (MCD_GHSL) to 84% (MUA_MCD) of all cities (Fig. 4(C)). It is worth noting that the annual daytime $\Delta SUHII_{RD}$ is greater than 50% in about 17% (MCD_GUB) to 34% (MUA_GUB) of all cities (Fig. 4(C)). Besides, approximately 10% cities have an annual daytime $\Delta SUHII_{RD}$ larger than 100% (or even up to 200%, i.e., the sign of SUHII flips) (Fig. 4(C)). On

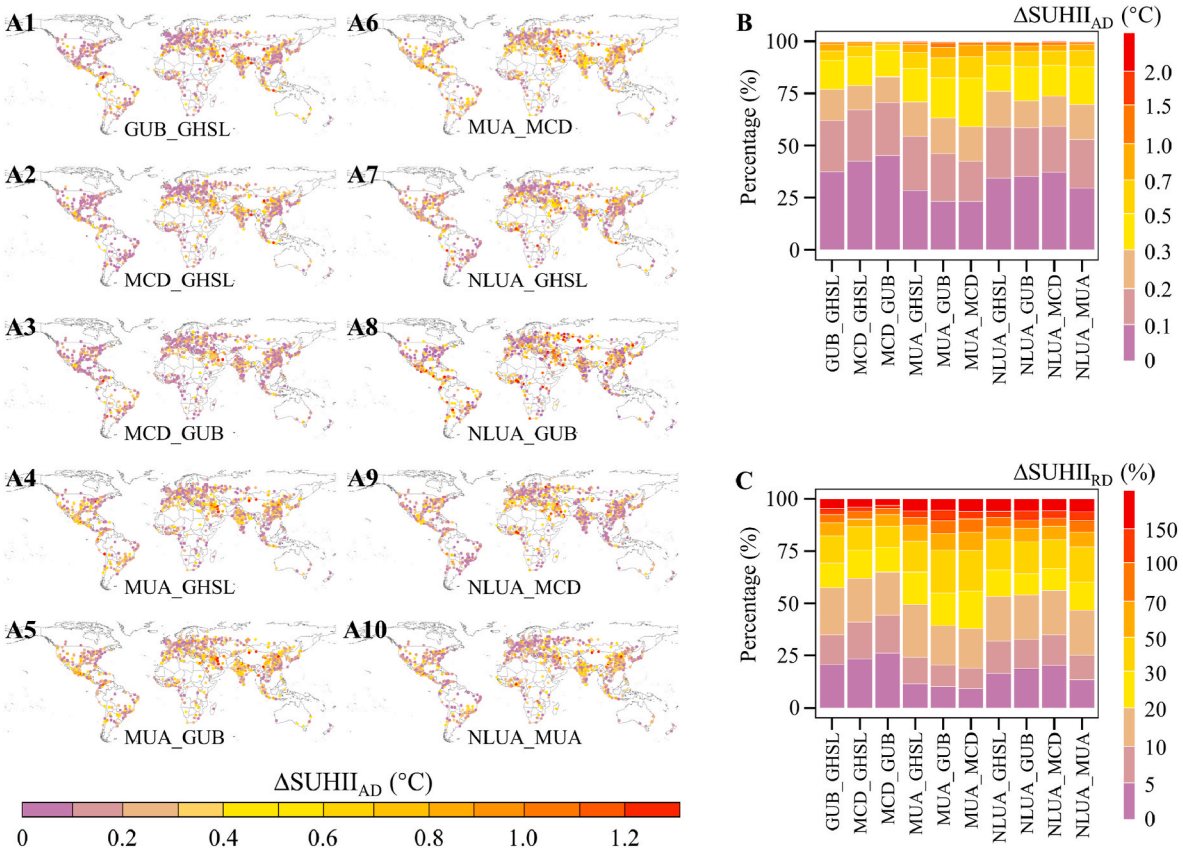

Fig. 5. Annual nighttime $\Delta SUHII_{AD}$ and $\Delta SUHII_{RD}$ for global cities. (A1-A10) Spatial distributions of $\Delta SUHII_{AD}$. (B) Stacked frequency distributions of $\Delta SUHII_{AD}$. (C) Stacked frequency distributions of $\Delta SUHII_{RD}$. $\Delta SUHII_{AD}$ and $\Delta SUHII_{RD}$ represent absolute and relative differences in SUHII between global urban extent products, respectively.

average for all cities, the annual daytime $\Delta SUHII_{RD}$ ranges from 30.8 ± 3.1% (MCD_GUB) to 52.2 ± 3.6% (MUA_GUB), with a mean value of 42.0 ± 2.7% (averages for all GUEP pairs) (Fig. 6(B1)).

The annual nighttime $\Delta SUHII_{AD}$ and $\Delta SUHII_{RD}$ appear to be smaller than that of annual daytime (Fig. 5 & Fig. A3). The vast majority of cities have an annual nighttime $\Delta SUHII_{AD}$ within 0.5 °C, accounting for 82% (MUA_MCD) to 96% (MCD_GUB) of all cities (Fig. 5(B)). On average for global cities, the annual nighttime $\Delta SUHII_{AD}$ has a minimum value of 0.17 ± 0.01 °C (MCD_GUB), a maximum value of 0.30 ± 0.02 °C (MUA_MCD), and a mean value of 0.24 ± 0.01 °C (averages for all GUEP pairs) (Fig. 6(A2)). In terms of the relative difference in SUHII, cities with an annual nighttime $\Delta SUHII_{RD}$ above 10% account for 55% (MCD_GUB) to 81% (MUA_MCD) of all cities (Fig. 5(C)). On average for all cities, the annual nighttime $\Delta SUHII_{RD}$ varies between 25.3 ± 2.5% (MCD_GUB) and 42.2 ± 3.1% (MUA_MCD), with a mean value of 35.2 ± 2.3% (averages for all GUEP pairs) (Fig. 6(B2)).

Fig. 7 shows the seasonal variations of the UED-induced uncertainty in SUHII estimates. The average daytime $\Delta SUHII_{AD}$ is highest during summer and lowest in winter, and a reverse seasonal pattern is observed for the average nighttime $\Delta SUHII_{AD}$. The situation changes when we consider the relative difference, and it is found that wintertime $\Delta SUHII_{RD}$ is stronger than summertime $\Delta SUHII_{RD}$ for both daytime and nighttime averages.

Figs. 8 and 9 show the spatiotemporal patterns of $\Delta SUHII_{AD}$ and $\Delta SUHII_{RD}$ in different climate zones. It is noted that the SUHII uncertainty caused by UED tends to be higher in cities located in the arid zone (Fig. 8). In the arid zone, the annual daytime and nighttime average $\Delta SUHII_{AD}$ values surpass the global averages, reaching 0.52 ± 0.05 °C and 0.31 ± 0.02 °C, respectively (Fig. 8(A)). More notably, the annual daytime $\Delta SUHII_{RD}$ for cities located in the arid zone averagely reaches a remarkable 60.8 ± 6.6%, nearly double that of other climatic zones (Fig. 8(B1)). In terms of seasonal variability, the patterns of the average $\Delta SUHII_{AD}$ and $\Delta SUHII_{RD}$ for each climatic zone are mostly similar to those of the global-scale averages (Fig. 9).

3.2. *Performance of the ISF-C method for reducing the UED-induced uncertainty in SUHII estimates*

Fig. 10 shows the histogram distributions of ΔDiffISF (i.e. difference in DiffISF among GUEPs) before and after processed by the ISF-C method. It can be seen that ΔDiffISF tends to be more concentrated around zero after using the ISF-C method. Due to the close relation between $\Delta SUHII_{AD}$ and ΔDiffISF (Fig. A4), the ISF-C method has the ability to reduce $\Delta SUHII_{AD}$. As depicted in Fig. 11, both $\Delta SUHII_{AD}$ and $\Delta SUHII_{RD}$ have been largely reduced after using the ISF-C method. On average for all GUEP pairs across global cities, the implementation of the ISF-C method has led to a reduction in the annual daytime $\Delta SUHII_{AD}$ ($\Delta SUHII_{RD}$) from 0.46 ± 0.02 °C (42.0 ± 2.7%) to 0.34 ± 0.02 °C (24.9 ± 2.4%). Likewise, the annual nighttime $\Delta SUHII_{AD}$ ($\Delta SUHII_{RD}$) has decreased from 0.24 ± 0.01 °C (35.2 ± 2.3%) to 0.19 ± 0.01 °C (23.0 ± 2.0%). These results imply the effectiveness of ISF-C method in reducing the UED-induced uncertainty in SUHII estimates.

Fig. 12 shows the sensitivity of $\Delta SUHII_{AD}$ and $\Delta SUHII_{RD}$ to the key parameter, ISF_U (i.e., the lower limit of ISF within urban extents), of the ISF-C method. Both $\Delta SUHII_{AD}$ and $\Delta SUHII_{RD}$ show a progressively decreasing trend as the ISF_U gradually increases from 0% to 75%. This suggests that a higher ISF_U could achieve a better effect of reducing the UED-induced uncertainty in SUHII estimates. Besides, it is found that the decreasing trend of $\Delta SUHII_{AD}$ and $\Delta SUHII_{RD}$ is gradually slowing down as the ISF_U increases. The alteration in $\Delta SUHII_{AD}$ and $\Delta SUHII_{RD}$ appears

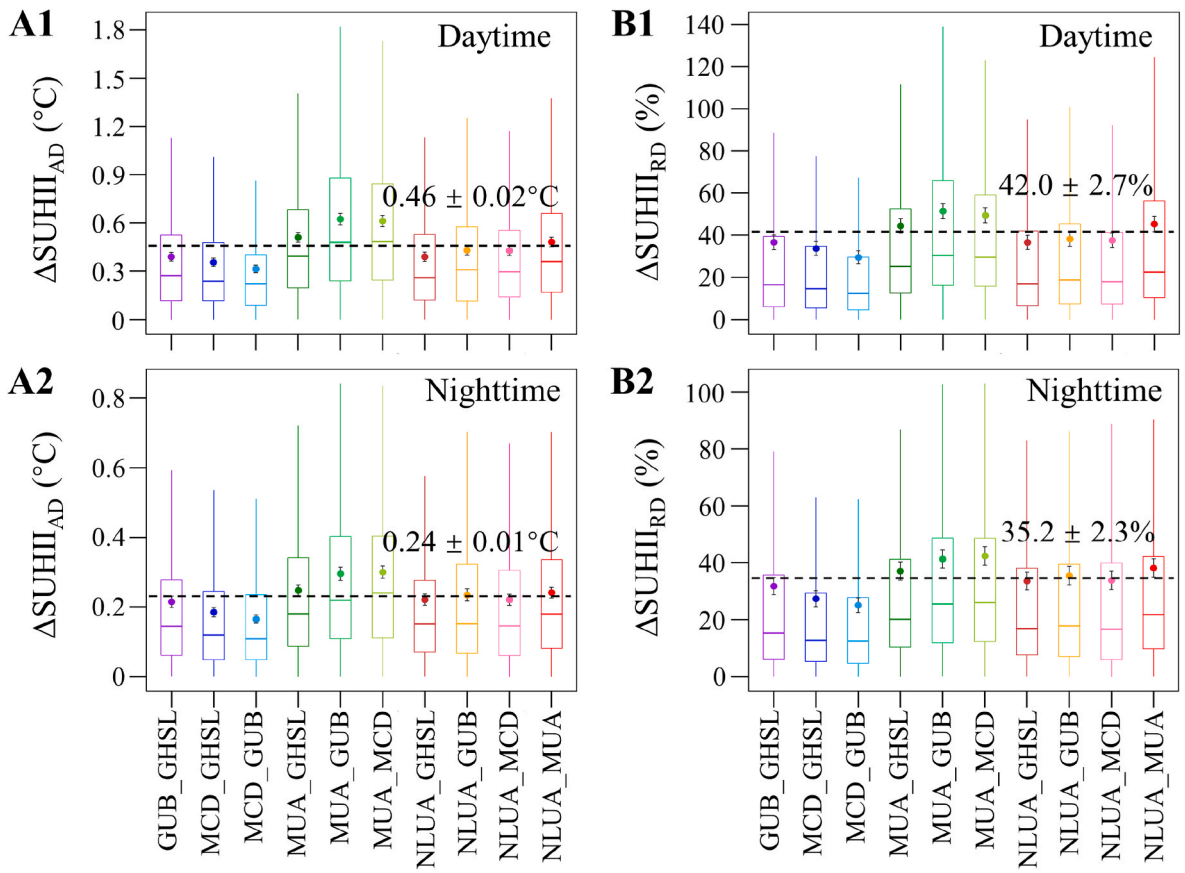

Fig. 6. Boxplots of $\Delta SUHII_{AD}$ and $\Delta SUHII_{RD}$ for global cities. (A1-A2) Annual daytime and nighttime $\Delta SUHII_{AD}$. (B1–B2) Annual daytime and nighttime $\Delta SUHII_{RD}$. $\Delta SUHII_{AD}$ and $\Delta SUHII_{RD}$ represent absolute and relative differences in SUHII between global urban extent products (GUEPs), respectively. The black dashed line and its above numbers (mean ± 95% confidence interval) represent the average $\Delta SUHII_{AD}$ or $\Delta SUHII_{RD}$ of all GUEP pairs. The central lines in the boxes are the median values. The colored circles and bars represent the mean values and 95% confidence intervals, respectively. Outliers are removed from the boxplot for presentation purposes.

to exhibit a notably slower pace when the ISF_U exceeds the value of 50%. However, it is also important to note that the increase in ISF_U can directly reduce the retained urban pixels for estimating SUHII (Fig. A5). Balancing the above two aspects, the ISF_U was therefore set to 50%, a commonly used threshold for the extraction of urban extents.

4. Discussion

4.1. Necessity for considering the UED-induced uncertainty in SUHII estimates

The quantification of the SUHI effect is a foundational aspect of urban thermal environment research. Presently, there are numerous methods available for estimating SUHII, primarily differing in the selection of urban and rural comparisons (Schwarz et al., 2011). In the majority of studies, urban areas are commonly delineated using current urban extent products, while rural reference areas are selected in close proximity to these urban areas (Chakraborty et al., 2022; Clinton and Gong, 2013; Du et al., 2021; Venter et al., 2021; Yao et al., 2019). There are also studies that categorize the city into different local climate zones (LCZs) based on the ground cover information and differentiate between urban and rural areas through LCZs (Bechtel et al., 2019; Stewart and Oke, 2012; Yang et al., 2020). Previous studies have extensively examined the SUHII uncertainty resulting from the rural definitions, and highlighted notable disparities in the estimated SUHII when employing different rural areas (Li et al. 2019a, 2022; Liu et al., 2023; Schwarz et al., 2011; Yang et al., 2023). This study focuses on the influence of discrepancy in urban extent on SUHII estimates, which has been rarely explored in previous studies.

The difference in urban extents can lead to variations in both the computed mean LST for urban areas and the computed mean LST for rural reference areas. The UED has led to average differences in urban mean LST (ΔLST_{Urban}) of 0.64 ± 0.03 °C and 0.35 ± 0.02 °C for annual daytime and nighttime, respectively (Fig. A. 6). Notably, these values exceed the corresponding UED-induced differences observed in rural reference areas (ΔLST_{Rural}), which are measured at 0.52 ± 0.03 °C and 0.28 ± 0.01 °C for annual daytime and nighttime, respectively (Fig. A. 6). This implies that discrepancy in urban mean LST could potentially play a more important role in accounting for the UED-induced uncertainty in SUHII estimates. Our results show that the global averages of the annual daytime and nighttime $\Delta SUHII_{RD}$ are as high as 42.0% and 35.2%, respectively (Fig. 6). In particular, about ten percent of cities have an annual daytime $\Delta SUHII_{RD}$ of more than 100%, and some cities even have an annual daytime $\Delta SUHII_{RD}$ of 200% (the sign of SUHII flips) (Fig. 4). Take Torreon, a city located in the arid zone, for example. For this city, the estimated annual daytime SUHII is negative when using the urban extent of GUB (−0.34 °C), MCD (−0.14 °C) or MUA (−0.13 °C), while it turns positive when based on the urban extent of GHSL (0.18 °C) or NLUA (0.01 °C) (Fig. 2). The similar situation also occurs in other cities such as Teheran, Luanda, and Tucson.

To summarize, differences in urban extents have an asymmetric impact on the average LST in urban and rural areas, which in turn introduces non-negligible uncertainty into the estimated SUHII. In the context of uncertainty analysis for SUHII estimates, our exploration of urban areas represents a noteworthy expansion upon existing studies that have predominantly focused on discrepancies in rural definitions (Li

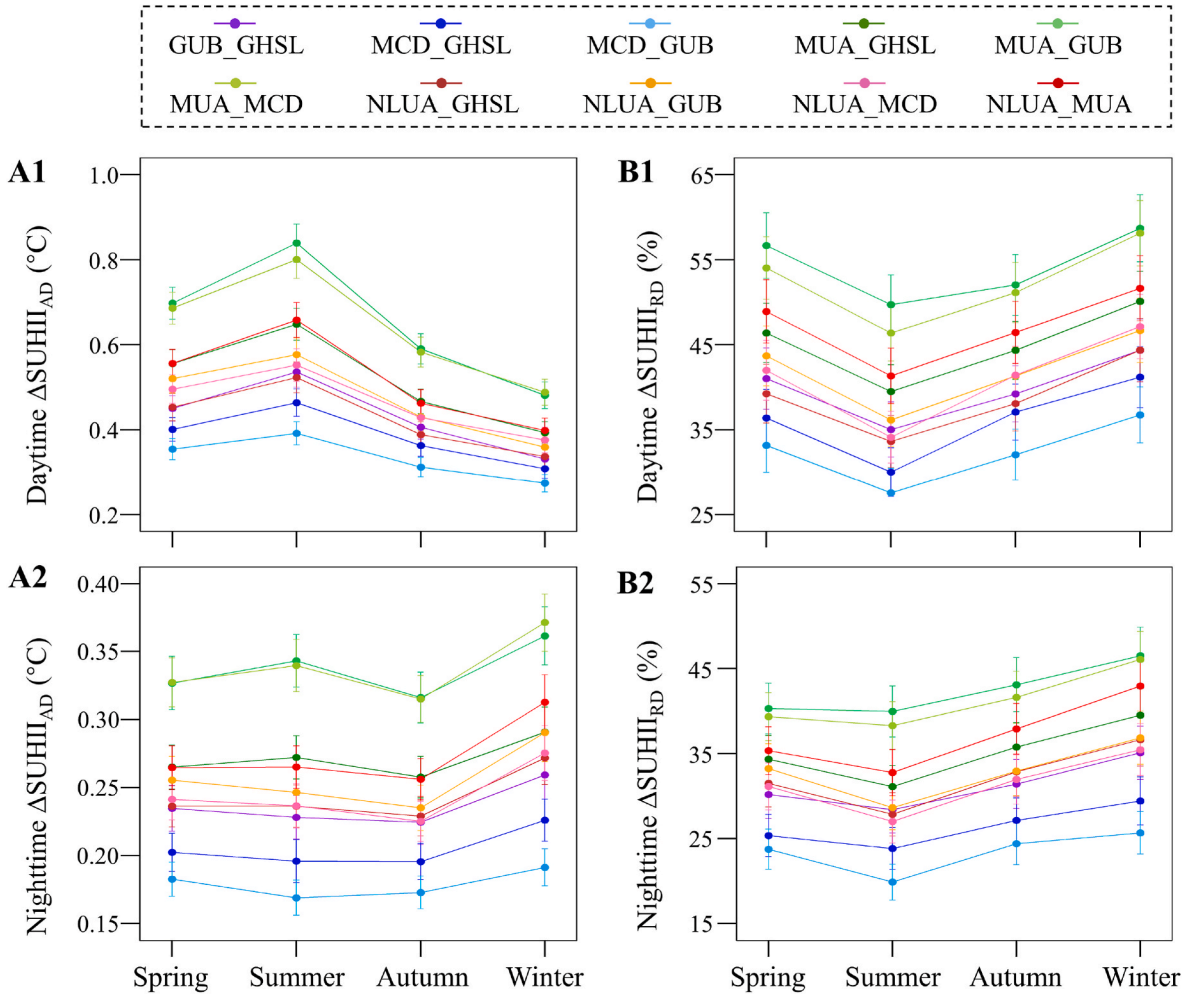

Fig. 7. Seasonal variations of $\Delta SUHII_{AD}$ and $\Delta SUHII_{RD}$ for global cities. (A1-A2) Annual daytime and nighttime $\Delta SUHII_{AD}$. (B1–B2) Annual daytime and nighttime $\Delta SUHII_{RD}$. $\Delta SUHII_{AD}$ and $\Delta SUHII_{RD}$ represent absolute and relative differences in SUHII between global urban extent products, respectively. The colored circles and bars represent the mean values and 95% confidence intervals, respectively.

et al. 2019a, 2022; Liu et al., 2023; Schwarz et al., 2011; Yao et al., 2018a). In a broader context, our study, together with previous research, collectively highlights the influence of quantification methods on SUHII estimates and helps to promote the standardization of SUHII quantification in the future.

4.2. Strategies for reducing the UED-induced uncertainty in SUHII estimates

Given the notable influence of UED on the estimation of SUHII, it becomes imperative to explore strategies for reducing the UED-induced uncertainty in SUHII estimates. The precise definition and extraction of urban extents is the most fundamental way to ensure the accuracy of SUHII estimates. However, current studies still have not reached a consensus on the definition or extraction of urban extents (Li et al., 2020b; Taubenböck et al., 2019; Zhao et al., 2022). Nowadays, there are numerous urban extent products available at both the regional scale and the global scale. Nevertheless, due to inconsistencies in the definition, data, and method for the extraction of urban extents, there exist differences in the urban extents corresponding to different products (Fig. 1). As a result, it is difficult for researchers to ensure the accuracy of the urban extents they use, leading to unpredictable uncertainties to the estimated SUHII.

Based on the above status, we proposed the ISF-C method, which is not bound to the accuracy of urban extents, but achieves to reducing the difference in SUHII corresponding to different GUEPs by imposing strict limits on the ISF within urban and rural extents. Moreover, Li et al. (2018) has introduced a method (referred as Li's method) for estimating SUHII by leveraging the inherent connection between LST and ISF with respect to their spatial distribution. Unlike our proposed ISF-C method, Li's method assumes a linear relationship between LST and ISF, and regards the linear regression coefficient of the two as the SUHII (i.e., the amount of change in LST corresponding to a 100% change in ISF). Li's method gets rid of the division between urban and rural areas, consequently reducing its susceptibility to the impact of urban extent discrepancies. Comparison demonstrates that Li's method can attain comparable effectiveness to ISF-C method in mitigating the SUHII uncertainty caused by UED (Fig. A7). However, the linear relationship between LST and ISF assumed by Li et al. (2018) might not hold true in some cities, due to the complexity of urban surface thermal environments (Fig. A8). This can hinder the broad applicability of the Li's method in these urban areas. In comparison, our proposed ISF-C method is more flexible and is expected to be applied in cities with more complex urban thermal environments. Besides, in cities where the linear relationship between LST and ISF is not well satisfied, the ISF-C method is somewhat better than Li's method at reducing the UED-induced uncertainty in SUHII estimates (Fig. A9). This further underscores the practical significance of our proposed ISF-C method.

Overall, this study not only provides a comprehensive examination of the influence of UED on the estimation of SUHII, but also introduces

Fig. 8. Boxplots of $\Delta SUHII_{AD}$ and $\Delta SUHII_{RD}$ for cities located in different climate zones. (A1-A2) Annual daytime and nighttime $\Delta SUHII_{AD}$. (B1–B2) Annual daytime and nighttime $\Delta SUHII_{RD}$. $\Delta SUHII_{AD}$ and $\Delta SUHII_{RD}$ represent absolute and relative differences in SUHII between global urban extent products (GUEPs), respectively. The colored numbers (mean ± 95% confidence interval) represent the average $\Delta SUHII_{AD}$ or $\Delta SUHII_{RD}$ of all GUEP pairs. The central lines in the boxes are the median values. The colored circles and bars represent the mean values and 95% confidence intervals, respectively. Outliers are removed from the boxplot for presentation purposes.

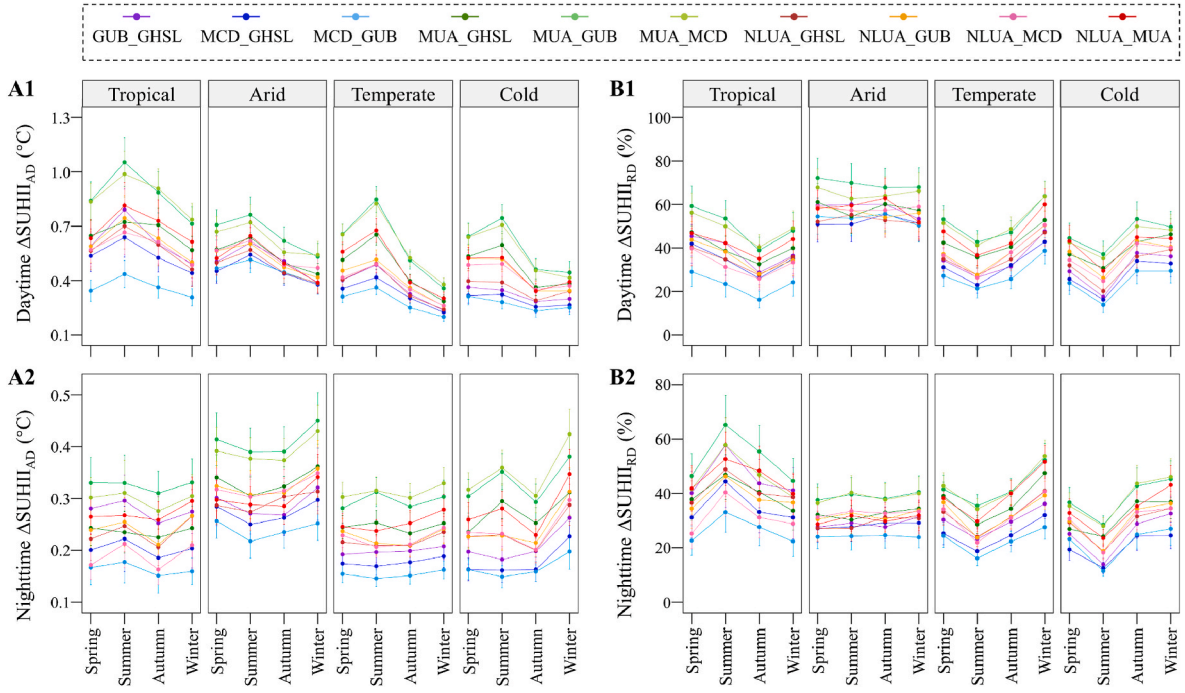

Fig. 9. Seasonal variations of $\Delta SUHII_{AD}$ and $\Delta SUHII_{RD}$ for cities located in different climate zones. (A1-A2) Seasonal variations of daytime and nighttime $\Delta SUHII_{AD}$. (B1–B2) Seasonal variations of daytime and nighttime $\Delta SUHII_{RD}$. $\Delta SUHII_{AD}$ and $\Delta SUHII_{RD}$ represent absolute and relative differences in SUHII among global urban extent products, respectively. The colored circles and bars represent the mean values and 95% confidence intervals, respectively.

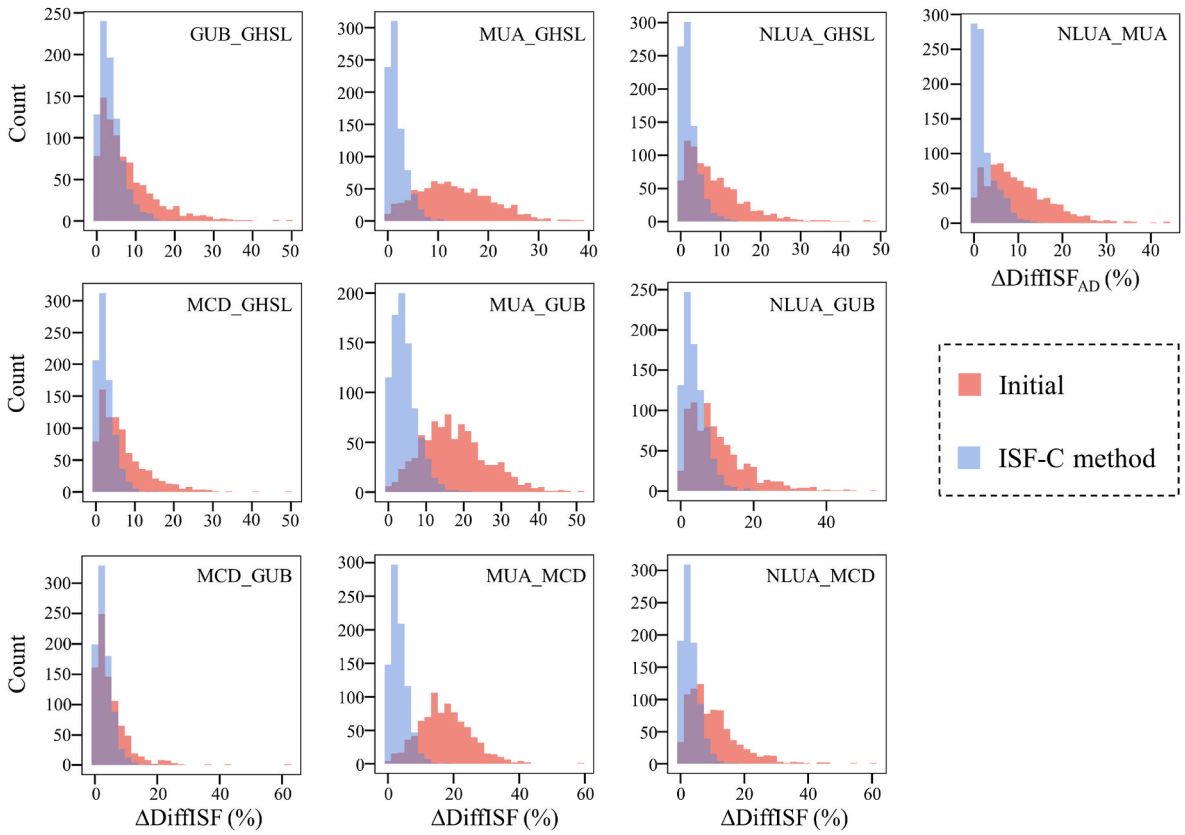

Fig. 10. Comparison of ΔDiffISF before and after processed by the ISF-C method. DiffISF is the urban-rural difference in mean impervious surface fraction (ISF), and ΔDiffISF represents the difference in DiffISF between global urban extent products.

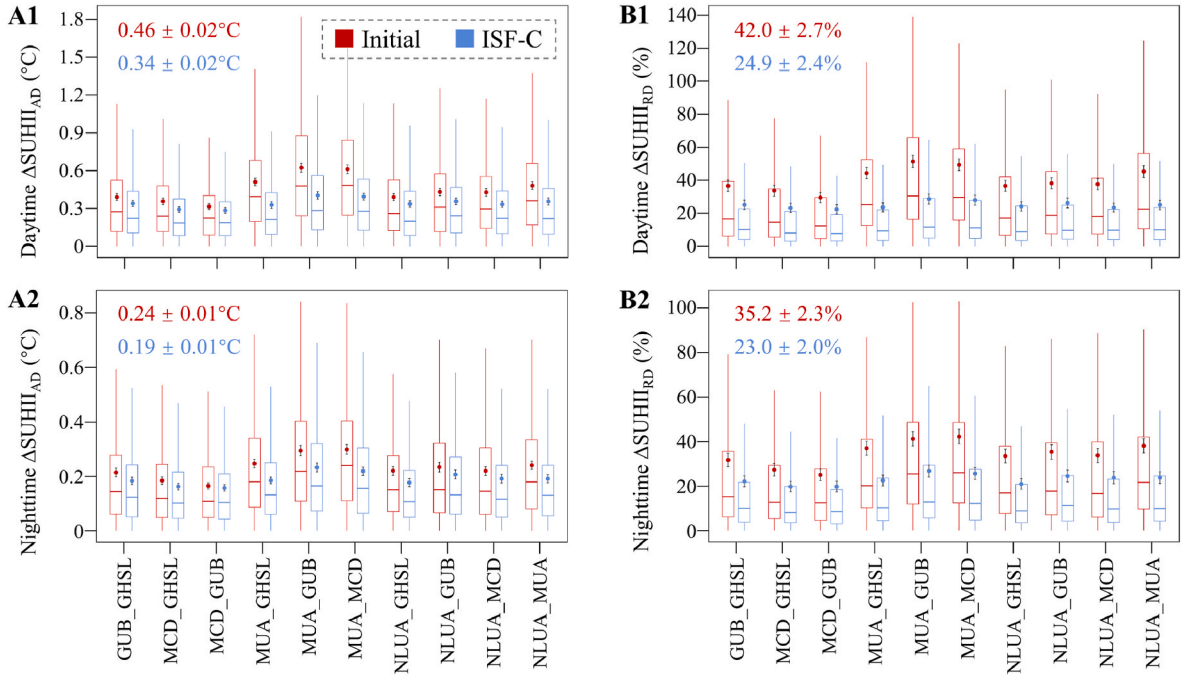

Fig. 11. ΔSUHII$_{AD}$ and ΔSUHII$_{RD}$ before and after processed by the ISF-C method. (A1-A2) Annual daytime and nighttime ΔSUHII$_{AD}$. (B1–B2) Annual daytime and nighttime ΔSUHII$_{RD}$. ΔSUHII$_{AD}$ and ΔSUHII$_{RD}$ represent absolute and relative differences in SUHII between global urban extent products (GUEPs), respectively. The colored numbers (mean ± 95% confidence interval) represent the average ΔSUHII$_{AD}$ and ΔSUHII$_{RD}$ of all GUEP pairs. The central lines in the boxes are the median values. The colored circles and bars represent the mean values and 95% confidence intervals, respectively. Outliers are removed from the boxplot for presentation purposes.

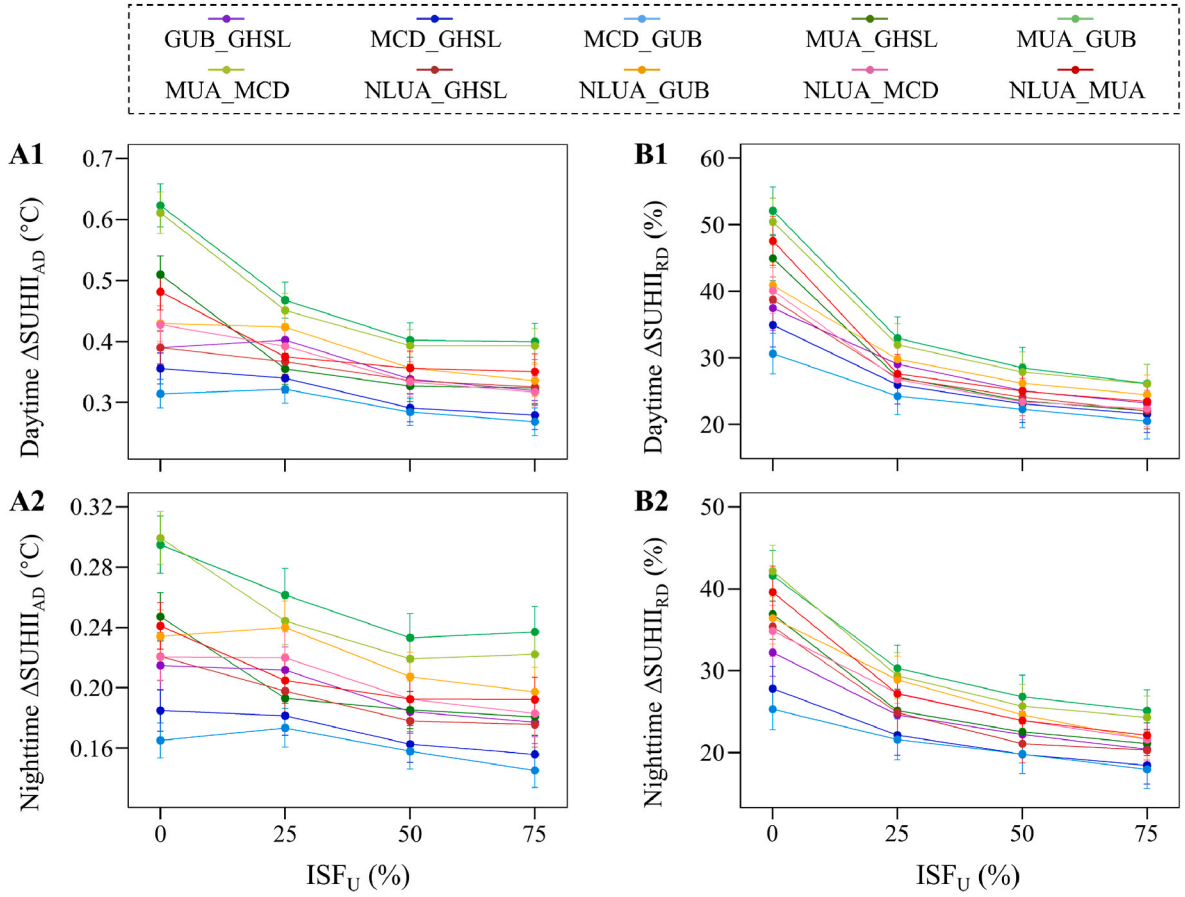

Fig. 12. Sensitivity of $\Delta SUHII_{AD}$ and $\Delta SUHII_{RD}$ to ISF_U of the ISF-C method. (A1-A2) Results of annual daytime and nighttime $\Delta SUHII_{AD}$. (B1–B2) Results of annual daytime and nighttime $\Delta SUHII_{RD}$. $\Delta SUHII_{AD}$ and $\Delta SUHII_{RD}$ represent absolute and relative differences in SUHII between global urban extent products, respectively. ISF_U represents the minimum impervious surface fraction (ISF) threshold of pixels that can be retained within urban extents. ISF_U is a key parameter of the ISF-C method, and please refer to Methods for more details about this method. The colored circles and bars represent the mean values and 95% confidence intervals, respectively.

the ISF-C method for reducing the UED-induced uncertainty in SUHII estimates. The ISF-C method stands out for its simplicity, effectiveness, and stability, presenting an alternative approach to alleviate the UED-induced uncertainty in SUHII estimates.

4.3. Limitations and future study

First, five commonly used and open-source GUEPs (i.e., global urban area products) were included in this study, and their corresponding SUHII differences were used to quantify the UED-induced uncertainty in SUHII estimates. These five GUEPs are from different sources, and differ in terms of definition, method, and data used for urban extent extraction. Therefore, the UED reflected by the differences among these five GUEPs is highly representative. However, as more urban extent products are produced and made freely available, future studies need to incorporate more data, which is important for a more comprehensive understanding of the UED-induced uncertainty in SUHII.

Second, this study focuses on the impact of difference in urban extent on SUHII estimates. However, there are various ways of defining the rural reference areas, and the difference in rural extents can also pose a significant influence on the estimation of SUHII (Li et al. 2019a, 2022; Liu et al., 2023; Schwarz et al., 2011). Future studies should try to explore the combined effect of urban extent discrepancy and rural definition difference on SUHII in order to gain a more in-depth understanding of how SUHII is quantified and its uncertainty.

Third, the ISF-C method has been proved to effectively reduce the UED-induced uncertainty in SUHII, but it also causes the reduction of available pixels within urban and rural extents. Besides, considering the uncertainty in satellite-derived surface properties, there are also inconsistencies in the distribution and accuracy of current ISF products (Huang et al., 2022). In this study, the effectiveness of the ISF-C method for reducing the UED-induced uncertainty in SUHII is verified by using the newly released high-resolution ISF products (Huang et al., 2022), and future studies should focus on impact of ISF differences on the ISF-C method.

Finally, all of our results utilize the MODIS MYD11A1 LST product. However, the magnitude of LST from different products (even different products derived from MODIS measurements) are inconsistent (Botje et al., 2022; Yao et al., 2020), which may also impact the SUHII estimates. Besides, remotely sensed LST images usually suffer from missing values due to the influence of clouds. Despite employing multi-images averaging, the variations in timing, location, and extent of LST data missing can introduce great uncertainties in the estimated SUHII (Hu and Brunsell, 2013; Li et al., 2022). Minimizing the uncertainty introduced by remotely sensed LST data in the estimation of SUHII is a focal challenge that warrants prioritization in future studies.

5. Conclusions

SUHII is the most typical indicator for studying the urban heat island effect, and its value relies on the definition of urban extents and their rural references. The impact of difference in the definition of the rural

reference on SUHII estimates has been widely explored, but the SUHII uncertainty caused by the UED still remains unclear. This study collected five commonly used and open-source GUEPs, and quantified the UED-induced uncertainty in SUHII estimates through comparing absolute SUHII difference (i.e., $SUHII_{AD}$) and relative SUHII difference (i.e., $SUHII_{RD}$) among GUEPs in 892 global cities. In addition, based on the strong relation between LST and ISF, the ISF-C method is proposed to reduce the SUHII difference between GUEPs by limiting the lower and upper limits of ISF within urban and rural extents, respectively.

The results show that the inconsistent urban extents delineated by different GUEPs lead to their difference in ISF as well as LST, which in turn causes uncertainties in the estimation of SUHII. On average for global cities, the mean values of annual daytime and nighttime $SUHII_{AD}$ for all GUEP pairs are 0.46 ± 0.02 °C and 0.24 ± 0.01 °C, respectively. Meanwhile, the mean values of annual daytime and nighttime $SUHII_{RD}$ for all GUEP pairs reach to $42.0 \pm 2.7\%$ and $35.2 \pm 2.3\%$, respectively. More notably, the annual daytime $\Delta SUHII_{RD}$ for cities located in the arid zone averagely reaches a remarkable $60.8 \pm 6.6\%$, which is nearly twice as high as that in other climate zones. Seasonal analysis shows that $\Delta SUHII_{AD}$ is generally higher in summer, and $\Delta SUHII_{RD}$ tends to be higher in winter. More importantly, both $\Delta SUHII_{AD}$ and $\Delta SUHII_{RD}$ show an obvious decreasing trend after processed by the ISF-C method, implying this method can serve to reduce the UED-induced uncertainty in SUHII estimates.

In conclusion, our study shows that the UED can have a non-negligible influence on SUHII estimates. Considering the inconsistency of urban extents among current products, researchers need to pay more attention to the possible bias caused by the urban extents themselves when estimating the SUHII. This study proposes a method to reduce the UED-induced uncertainty in SUHII estimates from the perspective of controlling the ISF within urban and rural extents, which can provide a valuable reference for future studies.

CRediT authorship contribution statement

Qiquan Yang: Conceptualization, Methodology, Investigation, Formal analysis, Visualization, Funding acquisition, Writing – original draft, Writing – review & editing. **Yi Xu:** Supervision, Funding acquisition, Writing – review & editing. **Xiaohua Tong:** Supervision, Funding acquisition, Writing – review & editing. **Ting Hu:** Conceptualization, Software, Writing – review & editing. **Yue Liu:** Writing – review & editing. **T.C. Chakraborty:** Writing – review & editing. **Rui Yao:** Writing – review & editing. **Changjiang Xiao:** Writing – review & editing. **Shurui Chen:** Writing – review & editing. **Zonghan Ma:** Writing – review & editing.

Declaration of competing interest

The authors declare that they have no known competing financial interests or personal relationships that could have appeared to influence the work reported in this paper.

Data availability

The MODIS daily LST products can be accessed from https://e4ftl01.cr.usgs.gov/MOLA/MYD11A1.061/. The Global Human Settlement Layer is available at https://ghsl.jrc.ec.europa.eu/download.php?ds=ucdb. The Global Urban Boundary dataset can be downloaded from http://data.starcloud.pcl.ac.cn/zh/resource/14. The MODIS land cover data is available from https://e4ftl01.cr.usgs.gov/MOTA/MCD12Q1.061/. The data link of the global Morphological Urban Area dataset is https://ars.els-cdn.com/content/image/1-s2.0-S0034425719303724-mmc1.zip. The global datasets of Nighttime-Light-based Urban Area can be accessed from https://figshare.com/articles/dataset/A_global_dataset_of_annual_urban_extents_1992-2020_from_harmonized_nighttime_lights/16602224/1. The global 30 arc-second elevation data can be downloaded from https://www.usgs.gov/centers/eros/science/usgs-eros-archive-digital-elevation-global-30-arc-second-elevation-gtopo30. The global impervious surface area is available at http://irsip.whu.edu.cn/. The global surface water data can be accessed from https://global-surface-water.appspot.com/download. The Köppen–Geiger climate map is available from http://www.gloh2o.org/koppen/. All data are available upon reasonable request from the authors.

Acknowledgment

This research was supported by the Macau Young Scholars Program (AM2022001), the Postdoctoral Science Foundation of China (2021TQ0245 and 2021M702470), the National Natural Science Foundation of China (42201389), and the Macao Science and Technology Development Fund (0049/2020/A1 and 0014/2022/A1). Pacific Northwest National Laboratory is operated for the U.S. Department of Energy (DOE) by Battelle Memorial Institute under contract DE-AC05-76RL01830. TC's contribution was supported by the COMPASS-GLM and ICoM projects. COMPASS-GLM is a multi-institutional project supported by DOE's Office of Science's Office of Biological and Environmental Research as part of the Earth and Environmental Systems Modeling program. ICoM is supported by the Regional and Global Modeling and Analysis program area of DOE.

Appendix A. Supplementary data

Supplementary data to this article can be found online at https://doi.org/10.1016/j.jclepro.2023.139032.

References

Bechtel, B., Demuzere, M., Mills, G., Zhan, W., Sismanidis, P., Small, C., Voogt, J., 2019. SUHI analysis using Local Climate Zones—a comparison of 50 cities. Urban Clim. 28.
Beck, H.E., Zimmermann, N.E., McVicar, T.R., Vergopolan, N., Berg, A., Wood, E.F., 2018. Present and future Koppen-Geiger climate classification maps at 1-km resolution. Sci. Data 5, 180214.
Botje, D., Dewan, A., Chakraborty, T.C., 2022. Comparing coarse-resolution land surface temperature products over Western Australia. Rem. Sens. 14, 2296.
Cao, C., Lee, X., Liu, S., Schultz, N., Xiao, W., Zhang, M., Zhao, L., 2016. Urban heat islands in China enhanced by haze pollution. Nat. Commun. 7, 12509.
Chakraborty, T., Lee, X., 2019. A simplified urban-extent algorithm to characterize surface urban heat islands on a global scale and examine vegetation control on their spatiotemporal variability. Int. J. Appl. Earth Obs. Geoinf. 74, 269–280.
Chakraborty, T., Sarangi, C., Lee, X., 2021. Reduction in human activity can enhance the urban heat island: insights from the COVID-19 lockdown. Environ. Res. Lett. 16, 054060.
Chakraborty, T., Venter, Z.S., Qian, Y., Lee, X., 2022. Lower urban humidity moderates outdoor heat stress. AGU Adv. 3.
Chen, K., Huang, L., Zhou, L., Ma, Z., Bi, J., Li, T., 2015. Spatial analysis of the effect of the 2010 heat wave on stroke mortality in Nanjing, China. Sci. Rep. 5, 10816.
Clinton, N., Gong, P., 2013. MODIS detected surface urban heat islands and sinks: global locations and controls. Remote Sens. Environ. 134, 294–304.
Du, H., Zhan, W., Liu, Z., Li, J., Li, L., Lai, J., Miao, S., Huang, F., Wang, C., Wang, C., Fu, H., Jiang, L., Hong, F., Jiang, S., 2021. Simultaneous investigation of surface and canopy urban heat islands over global cities. ISPRS J. Photogrammetry Remote Sens. 181, 67–83.
Duan, S.-B., Li, Z.-L., Wu, H., Leng, P., Gao, M., Wang, C., 2018. Radiance-based validation of land surface temperature products derived from Collection 6 MODIS thermal infrared data. Int. J. Appl. Earth Obs. Geoinf. 70, 84–92.
Hu, J., Yang, Y., Zhou, Y., Zhang, T., Ma, Z., Meng, X., 2022. Spatial patterns and temporal variations of footprint and intensity of surface urban heat island in 141 China cities. Sustain. Cities Soc. 77, 103585.
Hu, L., Brunsell, N.A., 2013. The impact of temporal aggregation of land surface temperature data for surface urban heat island (SUHI) monitoring. Remote Sens. Environ. 134, 162–174.
Huang, X., Song, Y., Yang, J., Wang, W., Ren, H., Dong, M., Feng, Y., Yin, H., Li, J., 2022. Toward accurate mapping of 30-m time-series global impervious surface area (GISA). Int. J. Appl. Earth Obs. Geoinf. 109, 102787.
Imhoff, M.L., Zhang, P., Wolfe, R.E., Bounoua, L., 2010. Remote sensing of the urban heat island effect across biomes in the continental USA. Remote Sens. Environ. 114, 504–513.
Jia, W., Zhao, S., 2019. Trends and drivers of land surface temperature along the urban-rural gradients in the largest urban agglomeration of China. Sci. Total Environ. 711, 134579.

Jin, M.S., 2012. Developing an index to measure urban heat island effect using satellite land skin temperature and land cover observations. J. Clim. 25, 6193–6201.
Kottek, M., Grieser, J., Beck, C., Rudolf, B., Rubel, F., 2006. World Map of the Köppen-Geiger climate classification updated. Meteorol. Z. 15, 259–263.
Lai, J., Zhan, W., Huang, F., Quan, J., Hu, L., Gao, L., Ju, W., 2018. Does quality control matter? Surface urban heat island intensity variations estimated by satellite-derived land surface temperature products. ISPRS J. Photogrammetry Remote Sens. 139, 212–227.
Li, H., Zhou, Y., Li, X., Meng, L., Wang, X., Wu, S., Sodoudi, S., 2018. A new method to quantify surface urban heat island intensity. Sci. Total Environ. 624, 262–272.
Li, J., Wang, F., Fu, Y., Guo, B., Zhao, Y., Yu, H., 2020a. A novel SUHI referenced estimation method for multicenters urban agglomeration using DMSP/OLS nighttime light data. IEEE J. Sel. Top. Appl. Earth Obs. Rem. Sens. 13, 1416–1425.
Li, K., Chen, Y., Gao, S., 2022. Uncertainty of city-based urban heat island intensity across 1112 global cities: background reference and cloud coverage. Remote Sens. Environ. 271, 112898.
Li, K., Chen, Y., Wang, M., Gong, A., 2019a. Spatial-temporal variations of surface urban heat island intensity induced by different definitions of rural extents in China. Sci. Total Environ. 669, 229–247.
Li, X., Gong, P., Zhou, Y., Wang, J., Bai, Y., Chen, B., Hu, T., Xiao, Y., Xu, B., Yang, J., Liu, X., Cai, W., Huang, H., Wu, T., Wang, X., Lin, P., Li, X., Chen, J., He, C., Li, X., Yu, L., Clinton, N., Zhu, Z., 2020b. Mapping global urban boundaries from the global artificial impervious area (GAIA) data. Environ. Res. Lett. 15, 094044.
Li, Y., Wang, L., Liu, M., Zhao, G., He, T., Mao, Q., 2019b. Associated determinants of surface urban heat islands across 1449 cities in China. Adv. Meteorol. 1–14, 2019.
Liu, H., He, B.-j., Gao, S., Zhan, Q., Yang, C., 2023. Influence of non-urban reference delineation on trend estimate of surface urban heat island intensity: a comparison of seven methods. Remote Sens. Environ. 296.
Liu, Y., Huang, X., Yang, Q., Cao, Y., 2021. The turning point between urban vegetation and artificial surfaces for their competitive effect on land surface temperature. J. Clean. Prod. 292, 126034.
Liu, Z., Zhan, W., Lai, J., Bechtel, B., Lee, X., Hong, F., Li, L., Huang, F., Li, J., 2022. Taxonomy of seasonal and diurnal clear-sky climatology of surface urban heat island dynamics across global cities. ISPRS J. Photogrammetry Remote Sens. 187, 14–33.
Miliaresis, G.C., Argialas, D.P., 1999. Segmentation of physiographic features from the global digital elevation model/GTOPO30. Comput. Geosci. 25, 715–728.
Mohsin, T., Gough, W.A., 2012. Characterization and estimation of urban heat island at Toronto: impact of the choice of rural sites. Theor. Appl. Climatol. 108, 105–117.
Pekel, J.-F., Cottam, A., Gorelick, N., Belward, A.S., 2016. High-resolution mapping of global surface water and its long-term changes. Nature 540, 418–422.
Peng, S., Piao, S., Ciais, P., Friedlingstein, P., Ottle, C., Breon, F.M., Nan, H., Zhou, L., Myneni, R.B., 2012. Surface urban heat island across 419 global big cities. Environ. Sci. Technol. 46, 696–703.
Rizwan, A.M., Dennis, L.Y.C., Liu, C., 2008. A review on the generation, determination and mitigation of Urban Heat Island. J. Environ. Sci. 20, 120–128.
Schwarz, N., Lautenbach, S., Seppelt, R., 2011. Exploring indicators for quantifying surface urban heat islands of European cities with MODIS land surface temperatures. Remote Sens. Environ. 115, 3175–3186.
Stewart, I.D., Oke, T.R., 2012. Local climate zones for urban temperature studies. Bull. Am. Meteorol. Soc. 93, 1879–1900.
Sun, Y., Wang, S., Wang, Y., 2020. Estimating local-scale urban heat island intensity using nighttime light satellite imageries. Sustain. Cities Soc. 57, 102125.
Taubenböck, H., Weigand, M., Esch, T., Staab, J., Wurm, M., Mast, J., Dech, S., 2019. A new ranking of the world's largest cities—do administrative units obscure morphological realities? Remote Sens. Environ. 232, 111353.
Venter, Z.S., Chakraborty, T., Lee, X., 2021. Crowdsourced air temperatures contrast satellite measures of the urban heat island and its mechanisms. Sci. Adv. 7, eabb9569.
Wan, Z., 2014. New refinements and validation of the collection-6 MODIS land-surface temperature/emissivity product. Remote Sens. Environ. 140, 36–45.
Wang, J., Georganos, S., Kuffer, M., Abascal, A., Vanhuysse, S., 2022. On the knowledge gain of urban morphology from space. Comput. Environ. Urban Syst. 95, 101831.
Yang, J., Zhan, Y., Xiao, X., Xia, J.C., Sun, W., Li, X., 2020. Investigating the diversity of land surface temperature characteristics in different scale cities based on local climate zones. Urban Clim. 34, 100700.
Yang, Q., Huang, X., Li, J., 2017. Assessing the relationship between surface urban heat islands and landscape patterns across climatic zones in China. Sci. Rep. 7, 9337–9347.
Yang, Q., Huang, X., Yang, J., Liu, Y., 2021. The relationship between land surface temperature and artificial impervious surface fraction in 682 global cities: spatiotemporal variations and drivers. Environ. Res. Lett. 16, 024032.
Yang, Q., Xu, Y., Tong, X., Huang, X., Liu, Y., Chakraborty, T., Xiao, C., Hu, T., 2023. An adaptive synchronous extraction (ASE) method for estimating intensity and footprint of surface urban heat islands: a case study of 254 North American cities. Remote Sens. Environ. 297, 113777.
Yao, R., Wang, L., Huang, X., Gong, W., Xia, X., 2019. Greening in rural areas increases the surface urban heat island intensity. Geophys. Res. Lett. 46, 2204–2212.
Yao, R., Wang, L., Huang, X., Niu, Y., Chen, Y., Niu, Z., 2018a. The influence of different data and method on estimating the surface urban heat island intensity. Ecol. Indicat. 89, 45–55.
Yao, R., Wang, L., Huang, X., Zhang, W., Li, J., Niu, Z., 2018b. Interannual variations in surface urban heat island intensity and associated drivers in China. J. Environ. Manag. 222, 86–94.
Yao, R., Wang, L., Wang, S., Wang, L., Wei, J., Li, J., Yu, D., 2020. A detailed comparison of MYD11 and MYD21 land surface temperature products in mainland China. Int. J. Digit. Earth 13, 1391–1407.
Zhang, P., Imhoff, M.L., Wolfe, R.E., Bounoua, L., 2014. Characterizing urban heat islands of global settlements using MODIS and nighttime lights products. Can. J. Rem. Sens. 36, 185–196.
Zhao, M., Cheng, C., Zhou, Y., Li, X., Shen, S., Song, C., 2022. A global dataset of annual urban extents (1992–2020) from harmonized nighttime lights. Earth Syst. Sci. Data 14, 517–534.
Zhou, B., Rybski, D., Kropp, J.P., 2017. The role of city size and urban form in the surface urban heat island. Sci. Rep. 7, 4791–4799.
Zhou, D., Xiao, J., Bonafoni, S., Berger, C., Deilami, K., Zhou, Y., Frolking, S., Yao, R., Qiao, Z., Sobrino, J., 2018. Satellite remote sensing of surface urban heat islands: progress, challenges, and perspectives. Rem. Sens. 11, 48.
Zhou, D., Zhang, L., Hao, L., Sun, G., Liu, Y., Zhu, C., 2016a. Spatiotemporal trends of urban heat island effect along the urban development intensity gradient in China. Sci. Total Environ. 544, 617–626.
Zhou, D., Zhao, S., Liu, S., Zhang, L., Zhu, C., 2014. Surface urban heat island in China's 32 major cities: spatial patterns and drivers. Remote Sens. Environ. 152, 51–61.
Zhou, D., Zhao, S., Zhang, L., Liu, S., 2016b. Remotely sensed assessment of urbanization effects on vegetation phenology in China's 32 major cities. Remote Sens. Environ. 176, 272–281.